CHEMISTRY

A customized MOF-polymer composite for rapid gold extraction from water matrices

Tianwei Xue[1]†, Tao He[2]†, Li Peng[1]*, Olga A. Syzgantseva[3], Ruiqing Li[1], Chengbin Liu[1], Daniel T. Sun[4], Guangkuo Xu[1], Rongxing Qiu[1], Yanliang Wang[1], Shuliang Yang[5]*, Jun Li[1]*, Jian-Rong Li[2]*, Wendy L. Queen[6]

With the fast-growing accumulation of electronic waste and rising demand for rare metals, it is compelling to develop technologies that can promotionally recover targeted metals, like gold, from waste, a process referred to as urban mining. Thus, there is increasing interest in the design of materials to achieve rapid, selective gold capture while maintaining high adsorption capacity, especially in complex aqueous-based matrices. Here, a highly porous metal-organic framework (MOF)–polymer composite, BUT-33–poly(*para*-phenylenediamine) (PpPD), is assessed for gold extraction from several matrices including river water, seawater, and leaching solutions from CPUs. BUT-33–PpPD exhibits a record-breaking extraction rate, with high Au^{3+} removal efficiency (>99%) within seconds (less than 45 s), a competitive capacity (1600 mg/g), high selectivity, long-term stability, and recycling ability. Furthermore, the high porosity and redox adsorption mechanism were shown to be underlying reasons for the material's excellent performance. Given the accumulation of recovered metallic gold nanoparticles inside, the material was also efficiently applied as a catalyst.

INTRODUCTION

With the ever-growing consumption of electronics and new energy industries, gold extraction via traditional virgin mining from ore is unable to meet the growing demand (*1*–*7*). Thus, it is imperative to complement virgin mining with the development of efficient routes to extract gold from nonconventional sources like electronic waste (e-waste) (*8*–*10*). For the recovery of gold from e-waste, adsorption technologies based on porous materials having an abundance of adsorption sites and fast gold removal from solutions have attracted much recent attention, resulting in a number of reports aimed at the extraction of gold from waste streams using a host of porous adsorbents such as metal-organic frameworks (MOFs) (*11*–*17*), covalent organic frameworks (*18*, *19*), porous aromatic frameworks (*20*), and porous polymers (*9*, *21*). Furthermore, it has been shown that postsynthetically functionalizing such porous materials with desired functionality is an effective strategy to prepare excellent adsorbents having high gold extraction capacity. However, some functionalization strategies also reduce the porosity of these porous materials sharply where the specific surface area can drop below 500 m^2/g (*13*–*15*, *19*), even below 50 m^2/g (*16*, *18*). Limited porosity can limit the exposure of adsorption sites, reducing the extraction rate and requiring hours or days to reach equilibrium. What is more, during the gold extraction process, gold often exists in complex water matrices (river water, seawater, e-waste leaching solution, etc.) with high concentrations of other interferents including competing metal ions and organic interferents. Thus, a material should be selective, stable over long term, and offer high gold capacity and removal efficiency in varied complex water matrices; however, reported adsorbents rarely evaluate their performance in complex matrices (*9*, *12*–*16*, *18*–*21*). This prompted us to explore the design of suitable porous adsorbents for the efficient and selective extraction of gold from different water matrices.

Here, a Ni(II)-pyrazolate (pz) MOF, Beijing University of Technology (BUT)–33, with ultrahigh porosity was rationally designed; given the material's large mesopores and excellent chemical stability, it was selected as a porous support for poly(*para*-phenylenediamine) (PpPD) (Fig. 1). The large internal surface area and suitable pore size of BUT-33 promoted a high polymer loading and more dispersed adsorption sites, leading to high adsorption capacity with outstanding removal rate for gold species from aqueous systems. This redox-active composite can also selectively extract gold from several complex matrices including river water, seawater, and leaching solution obtained from the computer central processing unit (CPU). Last, benefiting from the gold nanoparticles in situ generated by the redox-active polymer in the MOF, the gold-containing composite is found to be a highly efficient catalyst.

RESULTS

Synthesis and characterization of BUT-33–PpPD

To meet the requirements of adsorbents with rapid extraction speed, high removal rate, and excellent adsorption capacity in complex matrices, it is necessary to seek a proper host material that is highly porous and has immobilized and dispersed functional guests. On the basis of our previous report (*22*), BUT-33 with the sodalite-type net was synthesized using an ingeniously designed planar ligand, 2,4,6-tris[4-(pyrazolate-4-yl)phenyl]-1,3,5-triazine (H_3TPTA). Topologically, the period structure in BUT-33 consists of $TPTA^{3-}$ ligands and Ni_4pz_8 clusters in which each Ni(II) atom is linked to four N atoms of pyrazolate group in a square planar

[1]College of Chemistry and Chemical Engineering, Xiamen University, Xiamen, Fujian 361005, China. [2]Department of Environmental Chemical Engineering, Beijing University of Technology, Beijing 100124, China. [3]Department of Chemistry, Lomonosov Moscow State University, Moscow 119991, Russia. [4]The Molecular Foundry, Lawrence Berkeley National Laboratory, Berkeley, CA 94720, USA. [5]College of Energy, Xiamen University, Xiamen, Fujian 361102, China. [6]Institute of Chemical Sciences and Engineering, École Polytechnique Fédérale de Lausanne (EPFL), Rue de l'Industrie 17, Sion CH-1951, Switzerland.
†These authors contributed equally to this work.
*Corresponding author. Email: li.peng@xmu.edu.cn (L.P.); ysl@xmu.edu.cn (S.Y.); junnyxm@xmu.edu.cn (J.L.); jrli@bjut.edu.cn (J.-R.L.)

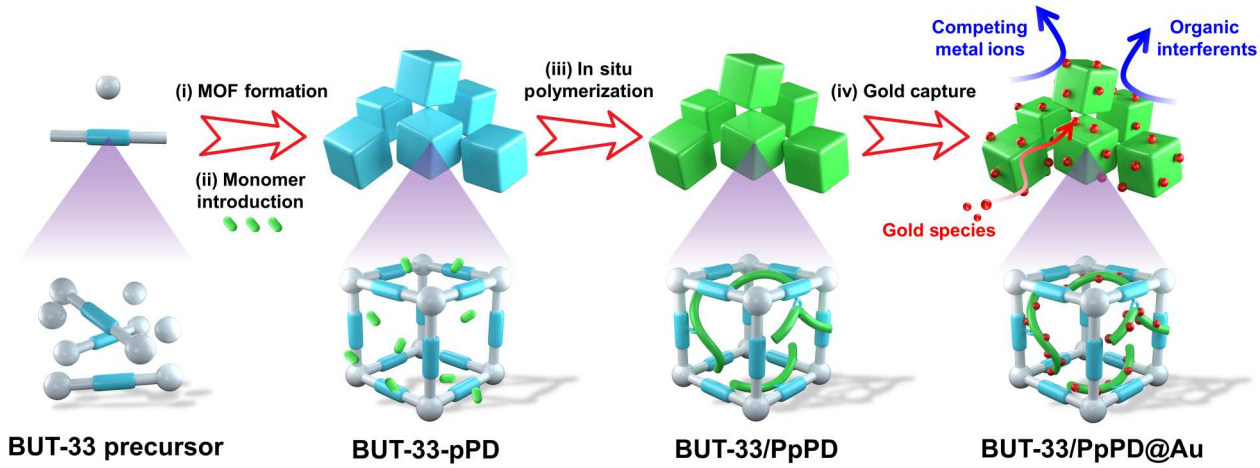

Fig. 1. Schematic illustration for the synthesis of BUT-33–PpPD and gold extraction.

geometry. Each square Ni_4pz_8 cluster coordinates to eight total $TPTA^{3-}$ ligands, thereby forming the the-a topological net (Fig. 2A). Each Ni(II) is undercoordinated, forming open metal sites, which can promote the polymerization of monomers. In the structure, eight $TPTA^{3-}$ linkers spreading over the faces and six Ni_4pz_8 clusters located at the vertices make up an octahedral cage, which forms a cavity having a diameter of 18.4 Å. These cages are arranged in a way that gives rise to another larger cavity having a diameter of 27.8 Å with open three-dimensional (3D) channels of aperture 22.4 Å, spreading along three crystallographic axial directions. Such a structure provides the space necessary for the polymerization of monomers and the accommodation of polymeric chains. The obtained MOF has a non-interpenetrated framework, providing a notable internal surface area of 4090 m^2/g and empty mesoporous cages of ~2.6 nm diameter (Fig. 2G and fig. S1) and open Ni(II) coordination sites, which offer a perfect platform for anchoring the polymer orderly in the MOF pores. The monomer, *para*-phenylenediamine (pPD), was selected because it can readily access the pores of BUT-33 for in situ polymerization and contains an abundance of amine groups (—NH_2), which promote the active sites for gold capture (*23*). Further, density functional theory (DFT) calculations were used to assess the feasibility of PpPD binding to Ni^{2+} sites (fig. S2 and table S1). The binding energies between the N of the monomer, dimer, and trimer and the Ni of BUT-33 indicate that the polymer has favorable interactions with the internal MOF surface. We believe that these interactions, combined with the unique cages containing open metal sites, allow the polymerization to occur throughout the MOF structure and readily become anchored inside, making polymer evenly disperse and tightly intertwine in MOF channels to expose more active sites and not easy to be lost in the actual application.

The in situ polymerization protocol was adapted for constructing MOF-polymer composite (*24*). In this case, 0.3 M pPD monomer and 20 mg of BUT-33 were used to prepare the MOF-polymer composite denoted as BUT-33–PpPD, which caused the MOF color change from yellow to dark gray (Fig. 2, B and C), indicating the successful formation of the highly conjugated polymer. Powder x-ray diffraction (PXRD) patterns show that, after polymerization, the structural integrity of BUT-33 was maintained (Fig. 2D). Scanning electron microscope (SEM) images indicate that the morphology of the MOF does not show obvious change, implying that most of polymer stays inside the pore (Fig. 2, E and F). Worth noting, nitrogen adsorption and desorption experiments demonstrate that the BET surface area of the composite after polymerization has decreased to 2743 m^2/g (Fig. 2G) because of the occupation of PpPD in the MOF pores, but this is still already higher than the surface areas of most MOFs, much less those that are functionalized with polymers (*25*–*28*). Further, the element analysis (table S2) and thermogravimetric analysis (fig. S3) indicated that ~18 wt % PpPD is found inside of BUT-33–PpPD. Compared to other three MOF-PpPD composites synthesized under the same conditions (table S3 and fig. S4), BUT-33–PpPD exhibits much higher surface area and contains larger amount of PpPD, which is one of the key factors for efficient gold capture. It indicates that the polymer host plays an important role in the MOF-polymer systems. Fourier transform infrared spectroscopy (FTIR) and Raman spectroscopy further indicate the structural integrity of BUT-33 (fig. S5). X-ray photoelectron spectroscopy (XPS) is used to probe the N 1s region of the BUT-33–PpPD spectrum (Fig. 2H). The peaks at 389.9, 400.0, and 401.9 eV are derived from =NR, R_2NH, and RNH_2, respectively, which confirm the existence of PpPD (*29*). Further, the matrix-assisted laser desorption/ionization time of flight mass spectrometry (MALDI-TOF-MS) of the digested BUT-33–PpPD sample also provides evidence of the polymerization of pPD and reveals oligomeric chains made up of seven monomeric units (fig. S6), which indicates that the MOF pore size limits the propagation of the polymer chain.

Adsorption performance with respect to Au-spiked water samples

Next, the performance of the composite for Au^{3+} recovery was evaluated. BUT-33–PpPD (5 mg) was soaked in different concentrations of Au^{3+} solutions [100 to 5000 parts per million (ppm)], and the maximum uptake of gold is found to be approximately 1600 mg/g (fig. S7), which is five times higher than that of the bare BUT-33 MOF, indicating that the functional groups on the polymer chains greatly enhance the gold capture. It is worth noting that composites with different loading amounts of the PpPD can be obtained by changing the concentration of monomer in the initial impregnation step. The adsorption

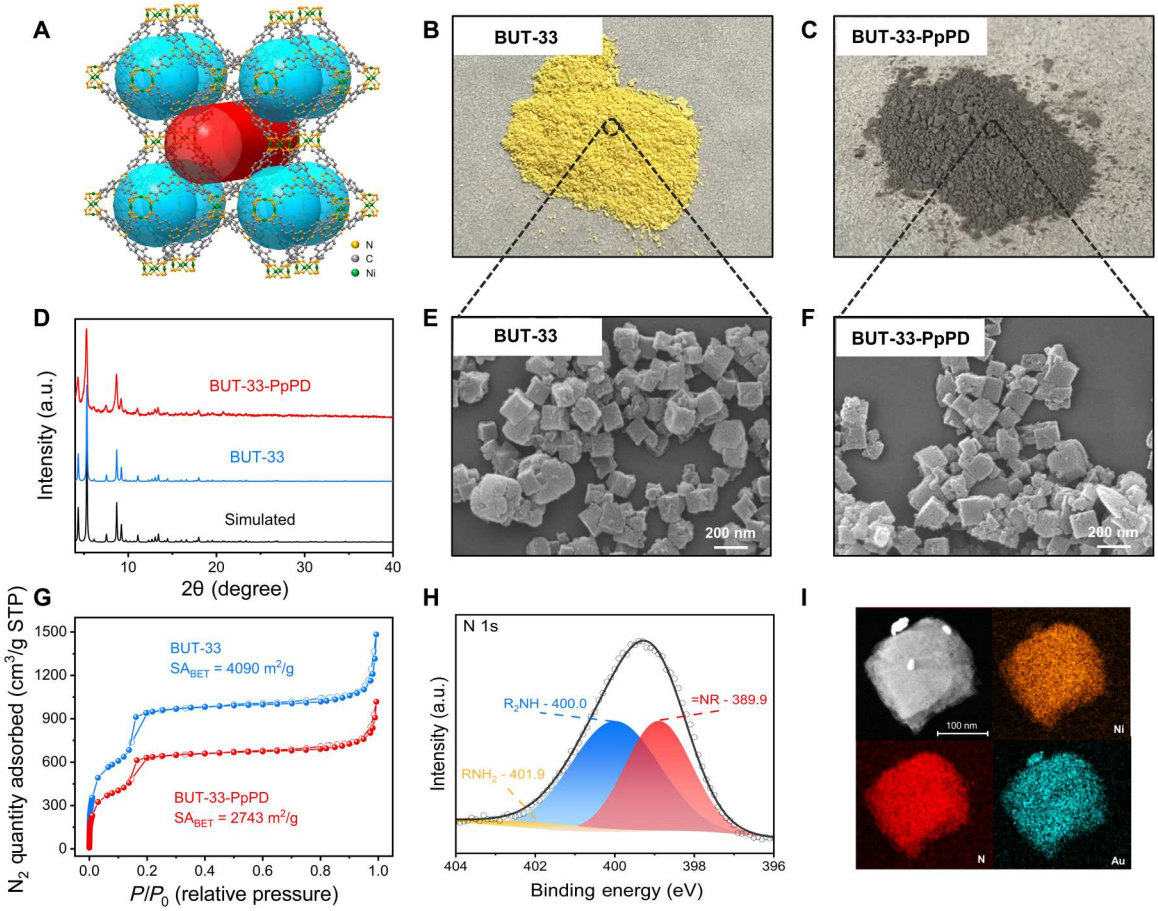

Fig. 2. Characterizations of BUT-33 and BUT-33–PpPD. (**A**) Structure of BUT-33 containing two kinds of pores. Sample pictures of (**B**) BUT-33 and (**C**) BUT-33–PpPD. (**D**) PXRD patterns of BUT-33 and BUT-33–PpPD compared to the simulated pattern of BUT-33. a.u., arbitrary units. SEM images of (**E**) BUT-33 and (**F**) BUT-33–PpPD. (**G**) N_2 adsorption and desorption isotherms for BUT-33 and BUT-33–PpPD. (**H**) N 1s x-ray photoelectron spectrum of BUT-33–PpPD. (**I**) HAADF-STEM image and corresponding EDX elemental maps from a slice of BUT-33–PpPD after gold adsorption.

capacities of these materials (5 mg) were measured in 10 ml of 1000 ppm Au^{3+} solutions over the course of 24 hours. When the quantity of gold extracted is plotted as a function of polymer loading, one observes a volcano-type curve (Fig. 3A), and the composite with 18% PpPD shows the highest adsorption capacity, which means that superfluous guest polymer molecules likely begin to block some pores, limiting the exposure of adsorption sites. Moreover, when the Au^{3+} adsorption capacity of several as-synthesized MOF-PpPD composites are compared, including Fe-BTC-PpPD, UiO-66-PpPD, MIL-127-PpPD (table S3), and other porous framework materials (table S4), BUT-33–PpPD has several advantages. For instance, the material exhibits an excellent adsorption capacity (1600 mg gold/g) and rapid extraction (Au^{3+} removal >99% within 45 s), which are among the best reported to date. This excellent performance could be ascribed to the ultrahigh porosity of BUT-33, which provides easy access to a large number of exposed adsorption sites.

Next, a simulated e-waste solution containing 10 ppm Au^{3+} and 100 ppm of common competitive ions was used to assess the selectivity, extraction kinetics, and acid/base stability of BUT-33–PpPD. Na^+, Mg^{2+}, Ca^{2+}, and K^+ were carefully selected because they are commonly found in surface water, while Ni^{2+}, Zn^{2+}, and Cu^{2+} are often found in leaching solutions of e-waste (Fig. 3B). For this solution, the removal percentage of Au^{3+} for BUT-33 is only about 60%, while BUT-33–PpPD removed over 99% Au^{3+} without obvious adsorption of other competing metal ions (Fig. 3C); this indicates that the introduction of PpPD polymer greatly enhances the gold scavenging ability of composite. The calculated distribution coefficient (K_d = 67,000) value of BUT-33–PpPD for Au^{3+} is 77 times that for Cu^{2+} and 280 times that for Ni^{2+}, which reflects the high affinity to gold of the designed BUT-33–PpPD (fig. S8). In addition, this composite achieves impressive gold uptake and simultaneously preserves the fast extraction speed observed for the host BUT-33. More than 90% of Au^{3+} is extracted under 15 s, more than 95% of Au^{3+} is extracted under 30 s, and more than 99% of Au^{3+} is extracted under 45 s (Fig. 3C), which is faster than that of other materials reported to date (tables S3 and S4 and fig. S9). To further evaluate the gold capture ability of the composite at low concentrations, 10 ml of solution with 1 ppm Au^{3+} was treated by 5 mg of BUT-33–PpPD, and inductively coupled plasma mass spectrometry (ICP-MS) showed that the concentration of Au^{3+} in the treated solution is lower than 0.1 parts per billion (ppb). Furthermore, it was observed that pH does not hinder the composite's extraction properties, and this composite maintains more than 99% removal

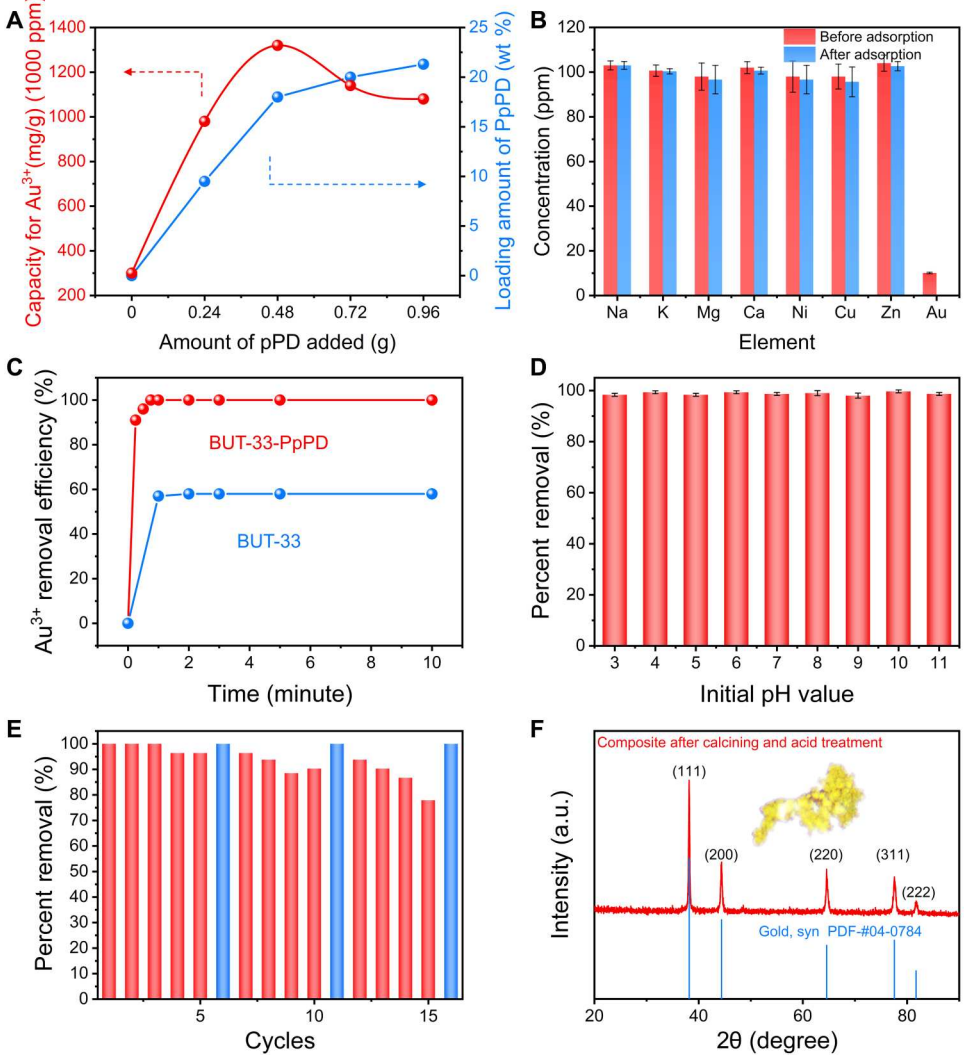

Fig. 3. Adsorption performance of BUT-33–PpPD in Au^{3+} solution. (**A**) Au^{3+} removal performance optimization for BUT-33–PpPD composites with different amounts of PpPD loading. (**B**) Selectivity adsorption of BUT-33–PpPD in solution with common competing metal ions. The concentration of metal ions before adsorption (red) and after adsorption (blue). (**C**) Extraction speed of BUT-33–PpPD and BUT-33. (**D**) Evaluation of adsorption performance of BUT-33–PpPD in solution with different initial pH values. (**E**) Evaluation of cyclability of adsorbent by ascorbic acid. Percent removal of Au^{3+} after multiple extractions (red) and regeneration cycles (blue). (**F**) PXRD pattern of BUT-33–PpPD after 15 cycles calcined at 900°C in air and subsequently treated with concentrated hydrochloric acid to recover metallic Au.

percentage for gold in solutions between pH 3 and 11 (Fig. 3D). Last but not least, the actual wastewater usually only contains a small amount of gold, requiring an adsorbent material to have the ability of recycling and regeneration to concentrate the gold from the solution. To evaluate the composite's cyclability, 20 mg of BUT-33–PpPD was added to 100 ml of a 100 ppm Au^{3+} solution. In the first three treatments, the removal percentage of gold can reach more than 99%, while in the next two cycles, the removal percentage gradually decreases, which is attributed to the oxidation and occupation of the N-containing functional active sites by the adsorbed Au species in the polymer. To regenerate the active sites, the composite was treated with 0.002 M neutralized ascorbic acid every five cycles, allowing the removal efficiency to recover. The results show that the composite could retain 99% removal after 15 cycles (Fig. 3E). After gold enrichment in the adsorbent, the composite was calcined at 900°C in the air to decompose the material and subsequently treated with concentrated hydrochloric acid to remove the dissolvable metal impurities for gold recovery. The PXRD patterns indicate that the final yellow solid is metallic gold (Fig. 3F). Then, the solid was digested with aqua regia and used for the ICP optical emission spectrometer (ICP-OES) test. Gold content exceeds 99%, and it does not contain other competing metals present in aqueous solutions.

Extraction of Au from complex water matrices

Because of gold scarcity, there are increasing numbers of reports making great efforts to design materials for gold recovery (table S4). For this, the performance of BUT-33–PpPD was assessed in several complex streams including river water and seawater. Consequently, 10 ppm of Au^{3+} and more than 150 ppm of Cu^{2+} and Ni^{2+} were added into the Yangtze River water (Nanjing, China) containing a large number of microorganisms, organic matter, and salts.

For this, 5 mg of BUT-33–PpPD was soaked in 10 ml of this solution. In less than 1 min, the composite extracted more than 99% of Au^{3+} and was almost not affected by the interfering substances (Fig. 4A and fig. S10A), possibly because the pores of BUT-33 act as a gatekeeper to prevent the larger interfering organic substance from approaching and blocking the adsorption sites, while smaller Au^{3+} can shuttle freely. The long-term stability of BUT-33–PpPD was also tested; for this, 20 mg of the composite was soaked in 100 ml of Yangtze River water. After 1 month, the PXRD patterns and SEM images confirm the structural and morphological integrity of BUT-33–PpPD (fig. S11, A and B). In addition, ICP-OES and MALDI-TOF-MS were applied to prove no loss of Ni or polymer (fig. S11, C and D). In view of the excellent performance of BUT-33–PpPD in river water, we next aimed to assess the material in an even more complex liquid. Seawater is considered one of the most complex liquid substrates on earth. It contains more than 80 elements, andsome of which are at ultrahigh concentrations. For example, the concentration of sodium ions can be as high as 10,000 ppm, which could seriously interfere with the efficiency of gold capture (*30*). To evaluate the performance of the composite in seawater, 5 mg of BUT-33–PpPD was treated with 10 ml of East China Sea water (Xiamen, China) spiked with 5.9 ppm Au^{3+}. Within 20 min, more than 99% of Au^{3+} was removed despite the complexity of the seawater (Fig. 4B and fig. S10B); this demonstrates that the material can function in highly complex environments, where there are large concentrations of competing ions.

Because of the ever-increasing demand for electronic devices, there is an accumulation of a large number of retired electronic devices (*31*). Although e-waste contains gold, copper, nickel, rare earth elements, and other materials, only about 17.4% of e-waste is currently recycled (*32*). It can be seen that there is a huge space for recovering the metals from the e-waste, and thus, effective

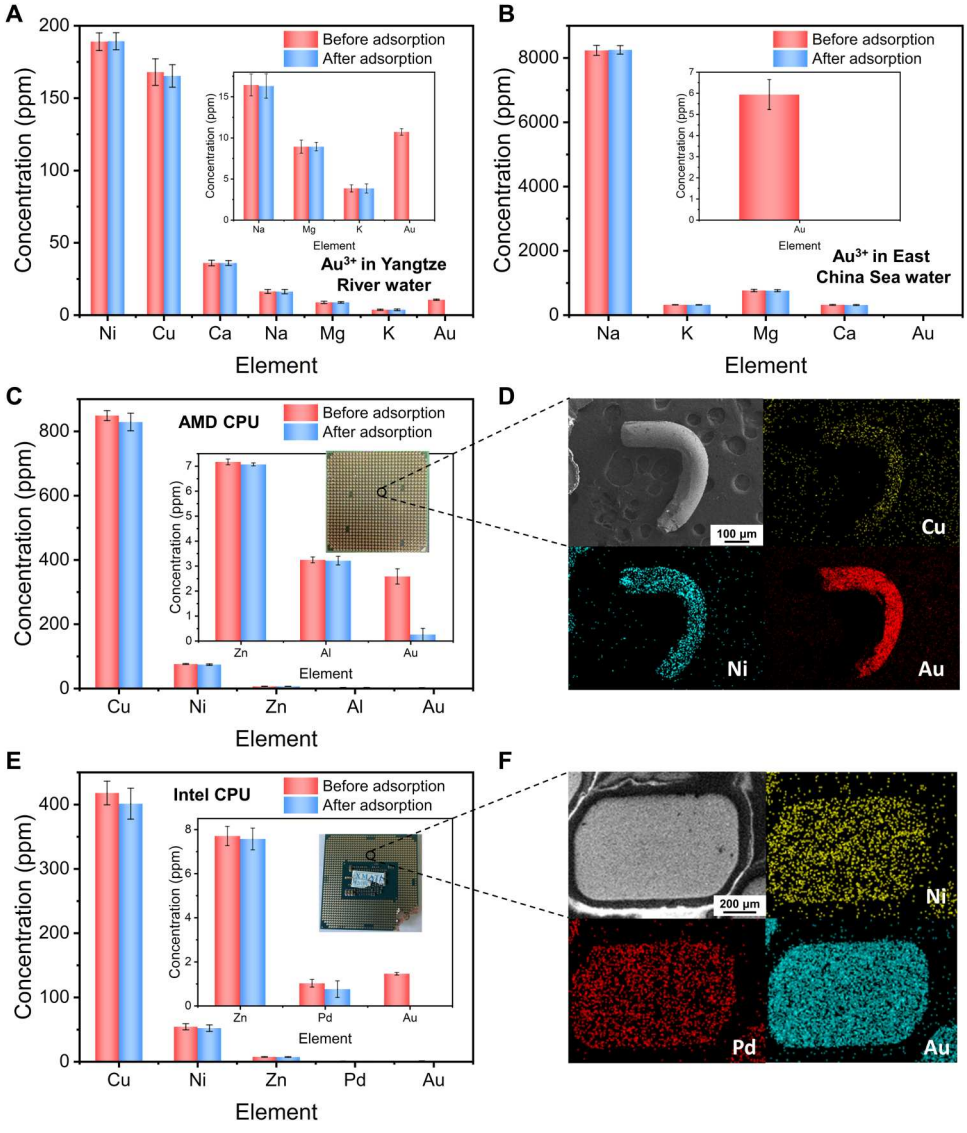

Fig. 4. Adsorption performance of BUT-33–PpPD in complex water matrices. The extraction of Au^{3+} in (**A**) Yangtze River water added with Au^{3+}, Ni^{2+}, and Cu^{2+}, (**B**) East China Sea water added with Au^{3+}, and leaching solution of (**C**) AMD CPU and (**E**) Intel CPU. SEM images and corresponding energy dispersive spectrometer (EDS) elemental maps from (**D**) AMD CPU and (**F**) Intel CPU.

adsorbents are highly desirable. With this in mind, the ability of this composite to extract gold from the real e-waste leaching solution was evaluated. Two electronics, AMD CPU (Fig. 4D) and Intel CPU (Fig. 4F), removed from abandoned computers were treated respectively by an aqueous solution of *N*-bromo succinimide and pyridine (fig. S12) (*33*), a simple and environmentally friendly method that can leach metals under neutral conditions. After dilution, the leaching solution of AMD CPU resulted in a 2.3 ppm Au solution also containing 850 ppm of Cu, 76 ppm of Ni, and small amounts of Zn and Al. Next, 10 ml of this solution was treated with 5 mg of BUT-33–PpPD, and more than 95% of gold was extracted in 5 min (Fig. 4C and fig. S10C). The leaching solution of the Intel CPU had a metal composition of 1.4 ppm of Au, 410 ppm of Cu, 53 ppm of Ni, 8 ppm of Zn, and 0.9 ppm of Pd. Following a similar treatment, >99% of gold was extracted in 5 min (Fig. 4E and fig. S10D). Although a small amount of Cu was also removed, the adsorption capacity is quite low. Furthermore, Cu is easily desorbed and dissolvable in HNO_3, and therefore, the purity of final gold will not be influenced.

Selective extraction mechanism of Au

To further understand the extraction mechanism, various characterization techniques were performed. It is expected that Au^{3+} ions interact with the nitrogen-containing active sites on PpPD in the BUT-33 pores, and then, Au^{3+} is subsequently reduced to gold with lower valence state by the redox-active polymer. The PXRD patterns of the material after extraction (denoted as BUT-33–PpPD@Au) indicate the presence of metallic gold (fig. S13A). The peaks at 38°, 42°, 65°, and 77° correspond to the (111), (200), (220), and (311) crystallographic planes of Au^0, respectively. According to the high-angle annular dark-field scanning transmission electron microscopy (HAADF-STEM) image and corresponding energy-dispersive x-ray (EDX) elemental maps of the serially sliced BUT-33–PpPD@Au composite crystals, it was observed that the gold is evenly distributed throughout the composite (Fig. 2I). Furthermore, the redox activity of PpPD was verified by XPS. The Au 4f region of the BUT-33–PpPD@Au spectrum demonstrates the existence of reduced Au^0 and Au^+ (fig. S13C). Moreover, the N 1s region of the BUT-33–PpPD@Au spectrum (fig. S13D) indicates that a great deal of RNH_2 and R_2NH groups is oxidized to =NR groups, confirming the redox adsorption mechanism in the gold capture process. The DFT calculations reveal that Au, in its oxidized and reduced state, forms a planar complex (Fig. 5A) with the PpPD chains, not distorting heavily their geometry. Such a nondistorted geometrical configuration is favorable for the effective adsorption of Au^{3+} by the BUT-33–PpPD composite, because it implies the preservation of MOF-polymer contacts and does not require their disruption. Considering the oxidation-reduction capacity of the pPD oligomer and polymer chains, it ranges within −5.2 to −6.5 eV, as estimated using corresponding monomers as the proxy (*34*) for the absolute energy-level alignment of PpPD. Hence, among all tested cations, it is suitable only for the reduction of Au^{3+}/Au^+ species (Fig. 5B). The redox potential of all other considered cations is too high for reduction by PpPD (*35*). Moreover, a suitable range of ionization potentials of oligomeric and polymeric pPD systems makes the reduction affordable in a wide range of pH, including the experimentally tested one between pH 3 and pH 11 (Fig. 5C). Therefore, both the favorable adsorption pattern and

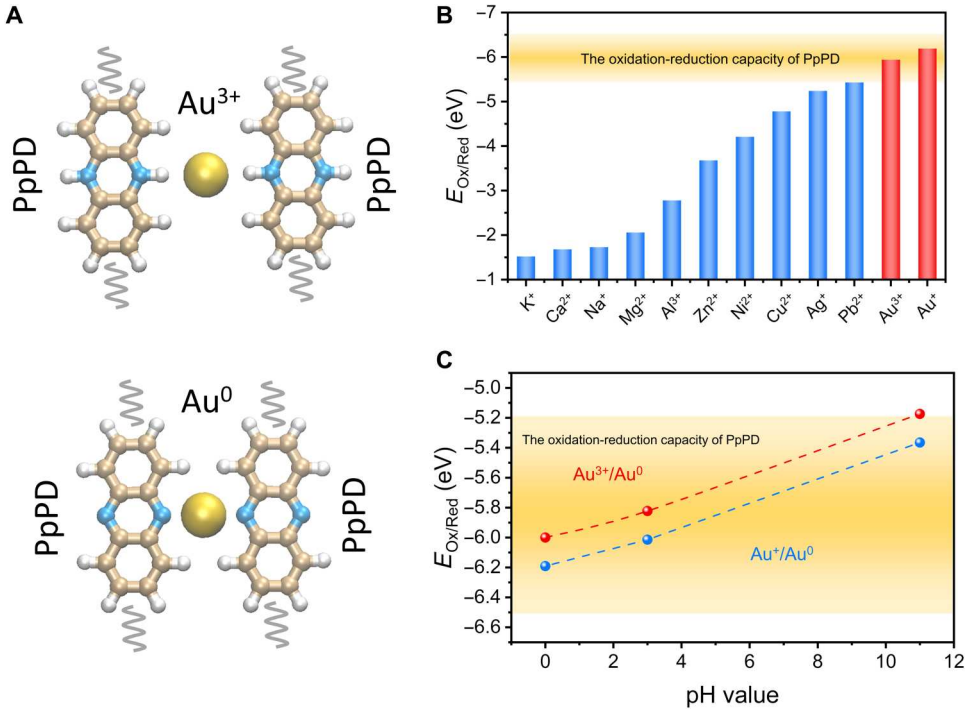

Fig. 5. DFT calculations for adsorption mechanism of Au. Physicochemical origins of the selectivity of BUT-33–PpPD toward Au. (**A**) Structures of the $Au^{3+/0}$-PpPD complexes. Au, C, N, and H atoms are colored gold, beige, blue, and white, respectively. (**B**) Redox potentials of Au^{3+}/Au^0, Au^+/Au^0 couples, and competing cations Cat^{n+}/Cat^0 (*47*). Favorable range of redox potentials, enabled by PpPD, is denoted in yellow. (**C**) pH dependence of redox potential for Au^{3+}/Au^0 and Au^+/Au^0 couples and its range favorable for reduction, enabled by PpPD and marked in yellow.

the suitable redox properties make PpPD-based composite an efficient material for selective Au^{3+} extraction from aqueous solutions.

This mechanism not only provides high selectivity for the composite but also skillfully saves the reduction step after gold concentration, allowing the material to be directly used in a number of appealing applications related to catalysis (*36*). To demonstrate this, the BUT-33–PpPD composite containing recovered Au was proven to act as an excellent catalyst candidate for the reduction of methylene blue and 4-nitrophenol, which has been a challenge in the field of environmental restoration (figs. S14 and S15).

DISCUSSION

Briefly, a MOF-polymer composite has been synthesized via in situ polymerization of pPD inside of a MOF, BUT-33. By properly selecting a MOF with an ultrahigh surface area (4090 m^2/g) and porosity as the polymer host, the resulting BUT-33–PpPD composite also displays a high surface area (2743 m^2/g). It is thought that the remaining porosity provides accessibility to a large quantity of metal-scavenging functionality on the polymer backbone. The composite is shown to rapidly and selectively extract gold from several highly complex aqueous matrices including river water, seawater, and leaching solutions of two different CPUs. The composite offers a notable adsorption capacity of 1600 mg/g, long-term stability in water, and recycling usability. The former is attributed to the redox-active sites of polymer, where Au^{3+} is reduced into its metallic state after adsorption. The resulting gold nanoparticles further afford the composite with catalytic activity. Overall, the composite's excellent performance helps to make a future case for the potential use of MOF-polymer composites in applications coupled to recycling and reusing targeted precious metals extracted from e-waste. The rational selection of MOF and polymer building blocks can allow us to fine-tune the resulting composites toward the selective separation of a number of different species from liquid and gas streams.

MATERIALS AND METHODS

Materials

All chemicals were used without further purification unless otherwise specified. *p*-Phenylenediamine, 4-bromobenzonitrile, and *tert*-butyl 4-(4,4,5,5-tetramethyl-1,3,2-dioxaborolan-2-*yl*)-1*H*-pyrazole-1-carboxylate were supplied by Energy Chemical. Gold trichloride and tetrakis(triphenylphosphine)palladium were bought from Sigma-Aldrich. 3,3′,5,5′-Azobenzene tetra carboxylic acid, trimesic acid, and terephthalic acid were purchased from Acmec. Sodium hydroxide, iron(III) chloride hexahydrate (97%), copper(II) nitrate trihydrate (99%), nickel(II) nitrate hexahydrate (99%), sodium nitrate (99%), magnesium(II) nitrate hexahydrate (99%), potassium nitrate, zinc(II) nitrate hexahydrate (99%), potassium carbonate, sodium carbonate, sodium sulfate, and all solvents were provided by Sinopharm Chemical Reagent Co. Ltd. The Yangtze River water was collected in Nanjing, China (latitude: 32.156613, longitude: 118.800723). The East China Sea water was collected in Xiamen, China (latitude: 24.442217, longitude: 118.075667).

Synthesis of BUT-33

H_3TPTA (0.40 mmol, 200 mg) was ultrasonically dissolved in 20 ml of *N*,*N*′-dimethylformamide (DMF) in a 15-ml high-pressure vessel. $Ni(OAc)_2{\cdot}4H_2O$ (0.60 mmol, 150 mg) was dissolved in 20 ml of DMF, then poured into the vessel, and mixed. The resulting mixture was then heated in an oil bath of 150°C for 2 hours, and a transformation from the green precipitate to a yellow solid was observed in the first 30 min of the reaction. After cooling down to room temperature, the yellow solid (155 mg of activated sample, 65% yield based on H_3TPTA) was collected by filtration, washed with DMF (3 × 50 ml) and acetone (3 × 50 ml), and dried under reduced pressure at 120°C.

Synthesis of BUT-33–PpPD

Twenty milligrams of BUT-33 were activated overnight at 125°C under a dynamic vacuum using a Schlenk line and an oil pump. After activation, it was cooled down to room temperature. A total of 0.48 g of pPD (0.24, 0.72, or 0.96 g; table S3 shows the relationship between adding amount of pPD and loading amount of PpPD in BUT-33) was dissolved in 20 ml of anhydrous methanol, which was loaded in a 50-ml round-bottom flask. The methanol solution was then transferred to the BUT-33–containing flask in an air-free way. The mixture was allowed to stir at 300 rpm for 1 hour. Then, the reaction was exposed to air and heated to 50°C for 24 hours. After cooling down to room temperature, the dark gray powder obtained was washed with methanol several times and dried under vacuum overnight for further use.

Characterization

PXRD was tested on Rigaku Ultima-IV X with a Cu Kα source (1.54056 Å) at 40 kV and 30 mA. All nitrogen adsorption measurements were performed on an ASAP 2020 HD88 instrument. XPS measurements were tested by Quantum 2000XPS with an Omicron hemispherical energy analyzer. SEM characterizations were performed on ZEISS Sigma. STEM images were collected by TECNAI F30, and corresponding STEM-EDX spectroscopy was performed. MALDI-TOF-MS analysis was performed using autoflex maX MALDI-TOF MS. FTIR spectra were collected using Nicolet iS50. The Raman data were collected using a Renishaw Invia instrument. The thermogravimetric analysis curve was obtained using TGA 449F5.

BUT-33–polymer interactions

DFT calculations were used to elucidate the interactions between BUT-33 and pPD. The periodic unit cell of BUT-33 is selected for DFT calculations. We chose some possible structures (one monomer, two dimers, and one trimer) to investigate the feasible binding configurations of the polymer to the MOF internal surface.

The DFT implemented in CP2K is based on a hybrid Gaussian plane wave scheme, the orbitals are described by an atom-centered Gaussian-type basis set, and an auxiliary plane wave basis set is used to reexpand the electron density in the reciprocal space. The 2s, 2p electrons of O, the 2s, 2p electrons of C, the 2s, 2p electrons of N, and the 3s, 3p, 3d, 4s electrons of Ni are treated as valence; the remaining core electrons are represented by Goedecker-Teter-Hutter (GTH) pseudopotentials. The Gaussian basis set of Ni is double-ζ with one set of polarization functions (DZVP), and others are triple-ζ with two sets of p-type or d-type polarization functions (TZV2P). The energy cutoff is set to 400 Ry. We use Perdew-

Burke-Ernzerhof (PBE) functions to describe the exchange-correlation effects, and the dispersion correction is applied in all calculations with the Grimme D3 method. Due to the large size of the cells, only the Γ point in the reciprocal space is used in our calculations. For geometry optimization, the Broyden-Fletcher-Goldfarb-Shanno (BFGS) minimizer is used.

The structure of BUT-33 is initially modeled with a cubic cell. The cells are optimized under 3D periodic boundary conditions. Possible adsorption conditions of chemical oxidation polymers of pPD are calculated. The binding energies (ΔE) of each configuration are determined as the difference energy difference before and after PpPD microparticles adsorbed, as shown in Eq. 1

$$\Delta E = E_{\mathrm{MOF+Poly}} - E_{\mathrm{MOF}} - E_{\mathrm{Poly}} \quad (1)$$

Au-PpPD interactions

To model Au-PpPD interactions, DFT calculations were performed. PpPD chain was represented by an oligomer in its reduced or oxidized form, containing either —NH— or —N═ sites. The Au^{3+} cation and Au^0 atom were positioned between two model polymer chains and allowed to fully relax. All the calculations are performed using the PBE density functional (*37*) along with Grimme′s D3 dispersion correction (*38*), as implemented in the CP2K package (*39*). The wave function was represented applying Gaussian-type double-ζ basis set (DZVP-MOLOPT) (*40*), while the electron density was expanded in the plane wave basis set with the 600-Ry cutoff. The core-valence interactions were described using norm-conserving GTH pseudopotentials (*41*). The range of PpPD ionization potentials was evaluated using the energies of highest occupied molecular orbital (HOMO) levels of pPD, computed at the DFT-B3LYP (*42*–*45*) level, as suitable monomeric proxy (*34*) for the assessment of the absolute energy-level alignment of polymeric PpPD chain. Structures are visualized with the VMD program (*46*).

Gold extraction

Following procedures previously described in (*11*), different concentrations of Au^{3+} solution were prepared using $AuCl_3$ and distilled water. Five milligrams of each sample was added to 10 ml of the aforementioned solution and was placed in a TCS10 constant temperature mixer at 800 rpm and held at a constant temperature of 25°C. The samples were allowed to shake for 24 hours to allow equilibrium. Afterward, the solutions were filtered using a 25-mm hydrophilic polytetrafluoroethylene (PTFE) membrane syringe filter with 0.22-μm pores to remove any solids for subsequent elemental analysis by ICP-OES. After analysis, the capacity, Q_e (mg/g), was calculated using Eq. 2

$$Q_e = \frac{(C_0 - C_e)V}{m} \quad (2)$$

where C_0 is the initial concentration, C_e is the equilibrium concentration, V is the volume, and m is the mass of the initially used composite.

Gold extraction in complex matrices

Following procedures previously described in (*11*), the composite selectivity for removing trace amounts of gold was evaluated. This was achieved by testing the materials′ performance in solution where other metal ions are up to 10 times the concentration of gold such as Na^+, Mg^{2+}, Ca^{2+}, K^+, Ni^{2+}, Zn^{2+}, and Cu^{2+}. What is more, the performance of composite in real-world samples was tested. First, water samples were obtained from the Yangtze River and spiked with 150 ppm of Cu and Ni and 10 ppm of Au. Afterward, 5 mg of each sample was added to 10 ml of the river water. For the pH study, the pH was adjusted using 0.02 M aqueous solutions of HNO_3 or NaOH. Five milligrams of BUT-33–PpPD were added after a desired pH was reached, and the pH was remeasured. Seawater was obtained from East China Sea and spiked with 5.9 ppm of Au. Afterward, 5 mg of each sample was added to 10 ml of the seawater.

All samples were placed in a TCS10 constant temperature mixer at 500 rpms and held at a constant temperature of 25°C. All samples were allowed to shake for 24 hours to allow equilibrium. Afterward, the solutions were filtered using a 25-mm hydrophilic PTFE membrane syringe filter with 0.22-μm pores to remove any solids for subsequent elemental analysis.

Gold extraction from leaching solution of AMD CPU and Intel CPU

The AMD and Intel CPUs were obtained from two abandoned computers in Xiamen University. Following procedures previously described in (*11*), the leaching solution was prepared by mixing 119.034 ml of distilled water with 0.966 ml of pyridine (100 mM) and 0.750 g of *N*-bromo succinimide (35 mM). Ten milliliters of this solution was used as the leaching solution and allowed to sit for 24 hours. Within hours, the leaching solution changed from clear to a blue solution and was diluted for subsequent elemental analysis. After the metal concentrations of competing metal ions and Au were determined, 5 mg of BUT-33–PpPD was added to 10 ml of the leaching solution and allowed to sit for 30 min.

All samples were placed in a TCS10 constant temperature mixer at 500 rpms and held at a constant temperature of 25°C. All samples were allowed to shake for 24 hours to allow equilibrium. Afterward, the solutions were filtered using a 25-mm hydrophilic PTFE membrane syringe filter with 0.22-μm pores to remove any solids for subsequent elemental analysis.

Gold extraction speed

Fifty milliliters of water spiked with 100 ppm of Na^+, Mg^{2+}, Ca^{2+}, K^+, Ni^{2+}, Zn^{2+}, Cu^{2+}, and 10 ppm of Au^{3+}, river water spiked with 150 ppm of Cu^{2+} and Ni^{2+} and 10 ppm of Au^{3+}, seawater spiked with 5.9 ppm of Au^{3+}, and leaching solution of two CPUs were treated by 5 mg of BUT-33–PpPD. At each time point (15, 30, and 45 s and 1, 2, 3, 5, 10, 15, 20, and 30 min), the aqueous samples were isolated and filtered using a 25-mm hydrophilic PTFE membrane syringe filter with 0.22-μm pores for subsequent elemental analysis.

Gold cycling and regeneration

Following procedures previously described in (*11*), cyclability of the composite was investigated using ascorbic acid for the reduction of imines to amines. For this experiment, 20 mg of BUT-33–PpPD was exposed to 20 ml of a Yangtze River water solution spiked with 100 ppm of Au^{3+} for 10 min. After exposure, the sample was centrifuged and the solution was filtered using a 25-mm hydrophilic PTFE membrane syringe filter with 0.22-μm pores. This process was repeated for five batches. After a clear drop in removal efficiency, the composite was soaked in 20 ml of a 0.002 M solution of

ascorbic acid for 4 hours, washed with methanol, and then exposed to another five batches. This protocol was repeated for a total of 16 batches of exposures.

Supplementary Materials

This PDF file includes:

Supplementary Text
Figs. S1 to S20
Tables S1 to S4
References

REFERENCES AND NOTES

1. R. A. Kerr, Mineral resources is the world tottering on the precipice of peak gold? *Science* **335**, 1038–1039 (2012).
2. Gold Demand Trends Q1 2022; www.gold.org/goldhub/research/gold-demand-trends/gold-demand-trends-q1-2022.
3. Gold Spot Prices; www.gold.org/goldhub/data/gold-prices.
4. K. Ueno, T. Oshikiri, Q. Sun, X. Shi, H. Misawa, Solid-state plasmonic solar cells. *Chem. Rev.* **118**, 2955–2993 (2018).
5. Gold Demand Hits Highest Level in More Than Two Years; www.gold.org/news-and-events/press-releases/gdt-full-year-2021-press-release.
6. W. Q. Liu, L. O. Jones, H. Wu, C. L. Stern, R. A. Sponenburg, G. C. Schatz, J. F. Stoddart, Supramolecular gold stripping from activated carbon using α-cyclodextrin. *J. Am. Chem. Soc.* **143**, 1984–1992 (2021).
7. R. L. Lin, Y. P. Dong, M. Tang, Z. C. Liu, Z. Tao, J. X. Liu, Selective recovery and detection of gold with cucurbit[*n*]urils (n = 5–7). *Inorg. Chem.* **59**, 3850–3855 (2020).
8. X. L. Zeng, J. A. Mathews, J. H. Li, Urban mining of e-waste is becoming more cost-effective than virgin mining. *Environ. Sci. Technol.* **52**, 4835–4841 (2018).
9. T. S. Nguyen, Y. R. Hong, N. A. Dogan, C. T. Yavuz, Gold recovery from e-waste by porous porphyrin-phenazine network polymers. *Chem. Mater.* **32**, 5343–5349 (2020).
10. B. Deng, X. Wang, D. X. Luong, R. A. Carter, Z. Wang, M. B. Tomson, J. M. Tour, Rare earth elements from waste. *Sci. Adv.* **8**, eabm3132 (2022).
11. D. T. Sun, N. Gasilova, S. L. Yang, E. Oveisi, W. L. Queen, Rapid, selective extraction of trace amounts of gold from complex water mixtures with a metal-organic framework (MOF)/polymer composite. *J. Am. Chem. Soc.* **140**, 16697–16703 (2018).
12. L. Gao, C. Y. V. Li, K. Y. Chan, Z. N. Chen, Metal-organic framework threaded with aminated polymer formed in situ for fast and reversible ion exchange. *J. Am. Chem. Soc.* **136**, 7209–7212 (2014).
13. M. Mon, J. Ferrando-Soria, T. Grancha, F. R. Fortea-Perez, J. Gascon, A. Leyva-Perez, D. Armentano, E. Pardo, Selective gold recovery and catalysis in a highly flexible methionine-decorated metal-organic framework. *J. Am. Chem. Soc.* **138**, 7864–7867 (2016).
14. C. Wang, G. Lin, J. L. Zhao, S. X. Wang, L. B. Zhang, Enhancing Au(III) adsorption capacity and selectivity via engineering MOF with mercapto-1,3,4-thiadiazole. *Chem. Eng. J.* **388**, 124221 (2020).
15. Z. Huang, M. H. Zhao, C. Wang, S. X. Wang, L. Q. Dai, L. B. Zhang, L. Xu, Selective removal mechanism of the novel Zr-based metal organic framework adsorbents for gold ions from aqueous solutions. *Chem. Eng. J.* **384**, 123343 (2020).
16. J. Y. Liu, Z. Deng, H. J. Yu, L. Wang, Ferrocene-based metal-organic framework for highly efficient recovery of gold from WEEE. *Chem. Eng. J.* **410**, 128360 (2021).
17. A. Kirchon, L. Feng, H. F. Drake, E. A. Joseph, H. C. Zhou, From fundamentals to applications: A toolbox for robust and multifunctional MOF materials. *Chem. Soc. Rev.* **47**, 8611–8638 (2018).
18. L. Zhang, Q. Q. Zheng, S. J. Xiao, J. Q. Chen, W. Jiang, W. R. Cui, G. P. Yang, R. P. Liang, J. D. Qiu, Covalent organic frameworks constructed by flexible alkyl amines for efficient gold recovery from leaching solution of e-waste. *Chem. Eng. J.* **426**, 131865 (2021).
19. H. L. Qian, F. L. Meng, C. X. Yang, X. P. Yan, Irreversible amide-linked covalent organic framework for selective and ultrafast gold recovery. *Angew. Chem. Int. Ed.* **59**, 17607–17613 (2020).
20. T. Ma, R. Zhao, Z. Li, X. Jing, M. Faheem, J. Song, Y. Tian, X. Lv, Q. Shu, G. Zhu, Efficient gold recovery from e-waste via a chelate-containing porous aromatic framework. *ACS Appl. Mater. Interfaces* **12**, 30474–30482 (2020).
21. Y. Hong, D. Thirion, S. Subramanian, M. Yoo, H. Choi, H. Y. Kim, J. F. Stoddart, C. T. Yavuz, Precious metal recovery from electronic waste by a porous porphyrin polymer. *Proc. Natl. Acad. Sci. U.S.A.* **117**, 16174–16180 (2020).
22. T. He, Z. H. Huang, S. Yuan, X. L. Lv, X. J. Kong, X. D. Zou, H. C. Zhou, J. R. Li, Kinetically controlled reticular assembly of a chemically stable mesoporous Ni(II)-pyrazolate metal–organic framework. *J. Am. Chem. Soc.* **142**, 13491–13499 (2020).
23. X. G. Li, M. R. Huang, W. Duan, Y. L. Yang, Novel multifunctional polymers from aromatic diamines by oxidative polymerizations. *Chem. Rev.* **102**, 2925–3030 (2002).
24. D. T. Sun, L. Peng, W. S. Reeder, S. M. Moosavi, D. Tiana, D. K. Britt, E. Oveisi, W. L. Queen, Rapid, selective heavy metal removal from water by a metal-organic framework/polydopamine composite. *ACS Cent. Sci.* **4**, 349–356 (2018).
25. T. Kitao, Y. Y. Zhang, S. Kitagawa, B. Wang, T. Uemura, Hybridization of MOFs and polymers. *Chem. Soc. Rev.* **46**, 3108–3133 (2017).
26. J. Canivet, A. Fateeva, Y. M. Guo, B. Coasne, D. Farrusseng, Water adsorption in MOFs: Fundamentals and applications. *Chem. Soc. Rev.* **43**, 5594–5617 (2014).
27. T. He, X.-J. Kong, Z.-X. Bian, Y.-Z. Zhang, G.-R. Si, L.-H. Xie, X.-Q. Wu, H. Huang, Z. Chang, X.-H. Bu, M. J. Zaworotko, Z.-R. Nie, J.-R. Li, Trace removal of benzene vapour using double-walled metal-dipyrazolate frameworks. *Nat. Mater.* **21**, 689–695 (2022).
28. P. Q. Liao, N. Y. Huang, W. X. Zhang, J. P. Zhang, X. M. Chen, Controlling guest conformation for efficient purification of butadiene. *Science* **356**, 1193–1196 (2017).
29. H. S. O. Chan, S. C. Ng, T. S. A. Hor, J. Sun, K. L. Tan, B. T. G. Tan, Poly(*m*-phenylenediamine): Synthesis and characterization by x-ray photoelectron spectroscopy. *Eur. Polym. J.* **27**, 1303–1308 (1991).
30. R. W. Ou, H. C. Zhang, V. X. Truong, L. Zhang, H. M. Hegab, L. Han, J. Hou, X. W. Zhang, A. Deletic, L. Jiang, G. P. Simon, H. T. Wang, A sunlight-responsive metal-organic framework system for sustainable water desalination. *Nat. Sustain.* **3**, 1052–1058 (2020).
31. International E-Waste Day: 57.4M Tonnes Expected in 2021; https://weee-forum.org/ws_news/international-e-waste-day-2021/.
32. Historical Demand and Supply; www.gold.org/goldhub/data/gold-demand-by-country.
33. C. L. Yue, H. M. Sun, W. J. Liu, B. B. Guan, X. D. Deng, X. Zhang, P. Yang, Environmentally benign, rapid, and selective extraction of gold from ores and waste electronic materials. *Angew. Chem. Int. Ed.* **56**, 9331–9335 (2017).
34. M. A. Syzgantseva, N. F. Stepanov, O. A. Syzgantseva, Band alignment as the method for modifying electronic structure of metal-organic frameworks. *ACS Appl. Mater. Interfaces* **12**, 17611–17619 (2020).
35. M. A. Syzgantseva, C. P. Ireland, F. M. Ebrahim, B. Smit, O. A. Syzgantseva, Metal substitution as the method of modifying electronic structure of metal-organic frameworks. *J. Am. Chem. Soc.* **141**, 6271–6278 (2019).
36. V. V. Karve, T. Schertenleib, J. Espin, O. Trukhina, X. Y. Zhang, M. X. Campins, T. Kitao, C. E. Avalos, T. Uemura, W. L. Queen, Hybridization of synthetic humins with a metal-organic framework for precious metal recovery and reuse. *ACS Appl. Mater. Interfaces* **13**, 60027–60034 (2021).
37. J. P. Perdew, K. Burke, M. Ernzerhof, Generalized gradient approximation made simple. *Phys. Rev. Lett.* **77**, 3865–3868 (1996).
38. S. Grimme, J. Antony, S. Ehrlich, H. Krieg, A consistent and accurate ab initio parametrization of density functional dispersion correction (DFT-D) for the 94 elements H-Pu. *J. Chem. Phys.* **132**, 154104 (2010).
39. T. D. Kuhne, M. Iannuzzi, M. Del Ben, V. V. Rybkin, P. Seewald, F. Stein, T. Laino, R. Z. Khaliullin, O. Schutt, F. Schiffmann, D. Golze, J. Wilhelm, S. Chulkov, M. H. Bani-Hashemian, V. Weber, U. Borstnik, M. Taillefumier, A. S. Jakobovits, A. Lazzaro, H. Pabst, T. Muller, R. Schade, M. Guidon, S. Andermatt, N. Holmberg, G. K. Schenter, A. Hehn, A. Bussy, F. Belleflamme, G. Tabacchi, A. Gloss, M. Lass, I. Bethune, C. J. Mundy, C. Plessl, M. Watkins, J. VandeVondele, M. Krack, J. Hutter, CP2K: An electronic structure and molecular dynamics software package - Quickstep: Efficient and accurate electronic structure calculations. *J. Chem. Phys.* **152**, 194103 (2020).
40. J. VandeVondele, J. Hutter, Gaussian basis sets for accurate calculations on molecular systems in gas and condensed phases. *J. Chem. Phys.* **127**, 114105 (2007).
41. S. Goedecker, M. Teter, J. Hutter, Separable dual-space Gaussian pseudopotentials. *Phys. Rev. B* **54**, 1703–1710 (1996).
42. K. Raghavachari, Perspective on "Density functional thermochemistry. III. The role of exact exchange". *Theor. Chem. Acc.* **103**, 361–363 (2000).
43. C. T. Lee, W. T. Yang, R. G. Parr, Development of the Colle-Salvetti correlation-energy formula into a functional of the electron density. *Phys. Rev. B* **37**, 785–789 (1988).
44. S. H. Vosko, L. Wilk, M. Nusair, Accurate spin-dependent electron liquid correlation energies for local spin density calculations: A critical analysis. *Can. J. Phys.* **58**, 1200–1211 (1980).
45. P. J. Stephens, F. J. Devlin, C. F. Chabalowski, M. J. Frisch, Ab initio calculation of vibrational absorption and circular dichroism spectra using density functional force fields. *J. Phys. Chem.* **98**, 11623–11627 (1994).
46. W. Humphrey, A. Dalke, K. Schulten, VMD: Visual molecular dynamics. *J. Mol. Graph. Model.* **14**, 33–38 (1996).

47. F. Macdonald, D. R. Lide, CRC handbook of chemistry and physics: From paper to web. *Abstr. Pap. Am. Chem. Soc.* **225**, –U552 (2003).
48. H. Chevreau, A. Permyakova, F. Nouar, P. Fabry, C. Livage, F. Ragon, A. Garcia-Marquez, T. Devic, N. Steunou, C. Serre, P. Horcajada, Synthesis of the biocompatible and highly stable MIL-127(Fe): From large scale synthesis to particle size control. *CrstEngComm* **18**, 4094–4101 (2016).
49. H. Furukawa, F. Gandara, Y. B. Zhang, J. C. Jiang, W. L. Queen, M. R. Hudson, O. M. Yaghi, Water adsorption in porous metal-organic frameworks and related materials. *J. Am. Chem. Soc.* **136**, 4369–4381 (2014).
50. S. Lin, D. H. K. Reddy, J. K. Bediako, M. H. Song, W. Wei, J. A. Kim, Y. S. Yun, Effective adsorption of $Pd_{(II)}$, $Pt_{(IV)}$ and $Au_{(III)}$ by $Zr_{(IV)}$-based metal-organic frameworks from strongly acidic solutions. *J. Mater. Chem. A* **5**, 13557–13564 (2017).
51. C. Wu, X. Y. Zhu, Z. Wang, J. Yang, Y. S. Li, J. L. Gu, Specific recovery and in situ reduction of precious metals from waste to create MOF composites with immobilized nanoclusters. *Ind. Eng. Chem. Res.* **56**, 13975–13982 (2017).
52. J. K. Guo, X. H. Fan, J. Y. Wang, S. H. Yu, M. W. Laipan, X. H. Ren, C. Zhang, L. Zhang, Y. T. Li, Highly efficient and selective recovery of Au(III) from aqueous solution by bisthiourea immobilized UiO-66-NH_2: Performance and mechanisms. *Chem. Eng. J.* **425**, 130588 (2021).

Acknowledgments: We thank L. Zhu and A. Chen for the help of Raman experiment and DFT calculation. We thank S. Xing for providing real-world samples. We also thank H. Wang, Y. Su, and Y. Hong for useful discussions. The research is carried out using the equipment of the shared research facilities of HPC computing resources at Lomonosov Moscow State University. The Siberian Branch of the Russian Academy of Sciences (SB RAS) Siberian Supercomputer Center is gratefully acknowledged for providing supercomputer facilities. **Funding:** This work was supported by National Natural Science Foundation of China grants 21903066 and 22078274 (to L.P. and J.L.) and President Fund of Xiamen University grant 20720210046 (to L.P.).
Author contributions: Conceptualization: W.L.Q., L.P., J.-R.L., J.L., and S.Y. Data curation: T.X. Formal analysis: T.X. and R.L. Funding acquisition: L.P. and J.L. Methodology: T.X., T.H., and O.A.S. Investigation: T.X., T.H., O.A.S., R.L., and C.L. Project administration: L.P. and J.L. Resources: L.P., J.L., and J.-R.L. Validation: C.L., G.X., and R.Q. Visualization: T.X. and O.A.S. Supervision: L.P., J.-R.L., J.L., and S.Y. Writing—original draft: T.X., T.H., O.A.S., G.X., and R.Q. Writing—review and editing: W.L.Q., L.P., J.-R.L., J.L., S.Y., D.T.S., and Y.W. **Competing interests:** The authors declare that they have no competing interests. **Data and materials availability:** All data needed to evaluate the conclusions in the paper are present in the paper and/or the Supplementary Materials.

Submitted 30 December 2022
Accepted 27 February 2023
Published 29 March 2023
10.1126/sciadv.adg4923